Available online at www.sciencedirect.com

SciVerse ScienceDirect

Ceramics International 38 (2012) 2129–2138

CERAMICS INTERNATIONAL

www.elsevier.com/locate/ceramint

Structural refinement, optical and microwave dielectric properties of $BaZrO_3$

S. Parida [a], S.K. Rout [a], L.S. Cavalcante [b,*], E. Sinha [a], M. Siu Li [c], V. Subramanian [d], N. Gupta [e], V.R. Gupta [e], J.A. Varela [b], E. Longo [b]

[a] Department of Applied Physics, Birla Institute of Technology, Mesra, Ranchi 835215, India
[b] Instituto de Química, UNESP, P.O. Box 355, 14801-907 Araraquara, SP, Brazil
[c] IFSC, Universidade de São Paulo, P.O. Box 369, 13560 970 São Carlos, SP, Brazil
[d] Department of Physics, Indian Institute of Technology Madras, Chennai 600036, India
[e] Department of Electronics and Communication Engineering, BIT Mesra, Ranchi 835215, Jharkhand, India

Received 6 August 2011; accepted 18 October 2011
Available online 26 October 2011

Abstract

In this work, barium zirconate ($BaZrO_3$) ceramics synthesized by solid state reaction method and sintered at 1670 °C for 4 h were characterized by X-ray diffraction (XRD), Rietveld refinement, and Fourier transform infrared (FT-IR) spectroscopy. XRD patterns, Rietveld refinement data and FT-IR spectra which confirmed that $BaZrO_3$ ceramics have a perovskite-type cubic structure. Optical properties were investigated by ultraviolet–visible (UV–vis) absorption and photoluminescence (PL) measurements. UV–vis absorption spectra suggested an indirect allowed transition with the existence of intermediary energy levels within the band gap. Intense visible green PL emission was observed in $BaZrO_3$ ceramics upon excitation with a 350 nm wavelength. This behavior is due to a majority of deep defects within the band gap caused by symmetry breaking in octahedral [ZrO_6] clusters in the lattice. The microwave dielectric constant and quality factor were measured using the method proposed by Hakki–Coleman. The dielectric resonator antenna (DRA) was investigated experimentally and numerically using a monopole antenna through an infinite ground plane and Ansoft's high frequency structure simulator software, respectively. The required resonance frequency and bandwidth of DRA were investigated by adjusting the dimension of the same material.

Keywords: A. Solid state reaction; B. Defects; C. Optical properties; D. Perovskites; E. Functional applications

1. Introduction

Ceramic materials with a perovskite-type structure have an extraordinary capacity for application in several functions such as displays, electronic/piezoelectric devices, sensors, actuators, transducers, and wireless communications [1–3]. Because of these diverse functions with direct technological applications, much research has been devoted to investigating different properties of barium zirconate ($BaZrO_3$) [4–7].

Among the perovskites with cubic structures, $BaZrO_3$ is a refractory ceramic material which is very promising due to its high melting point (2920 °C) and low chemical reactivity with corrosive compounds [8]; it is the sole ceramic material that does not follow phase transitions over the range from 1327 °C down to −269 °C [9]. In addition, $BaZrO_3$ has excellent thermal stability and resistance due to a low coefficient of thermal expansion ($\alpha = 87 \times 10^{-7}$/°C between 25 °C and 1080 °C) [10,11].

Recently, several literature studies have been reported on the PL properties of this perovskite (undoped and earth-rare doped) which are mainly due to its excellent optical properties [12–17]. In particular, these papers contain several theories on the wide band visible emission observed at room temperature which belongs to a universal ''green-luminescence''. The origin of green luminescence by different mechanisms has been explained and discussed in many papers, including the presence of localized electronic levels and a charge gradient in the band gap due to a symmetry break into lattice [18,19], intrinsic defects due to a change in shape and morphology [20,21], recombination of electrons and holes [22,23], oxygen vacancies

* Corresponding author. Tel.: +55 86 9808 4129; fax: +55 16 3361 8214; mobile: +55 16 8149 8182.
E-mail addresses: skrout@bitmesra.ac.in (S.K. Rout), laeciosc@bol.com.br (L.S. Cavalcante).

0272-8842/$36.00
doi:10.1016/j.ceramint.2011.10.054

[24], defects present in the lattice which lead to electronic transitions between the clusters and a correlation with ab initio calculations performed on the electronic structure for the formation of new levels between the valence band and the conduction band [25,26].

The microwave region of the electromagnetic spectrum has been of specialized interest for a long time. Due to the rapid development of technology for this frequency range, it has increasingly attracted attention in the past decades [27–29]. Some of the more obvious areas of intensive development strongly increased the demand for special dielectric materials (high dielectric constant and low loss) in the microelectronics industry as well as in short- and long-range communications [30]. Microwave dielectric materials play a key role in global society with a wide range of applications from terrestrial and satellite communications including software radio, global positioning system (GPS), and direct-broadcast satellite (DBS) TV to environmental monitoring via satellites [31]. The recent progress in microwave telecommunication, satellite broadcasting and intelligent transport systems (ITS) has resulted in an increasing demand for dielectric resonator antenna (DRA) which are low loss ceramic pucks used mainly in wireless communication devices [32]. The high dielectric constant and low loss in $BaZrO_3$ ceramics make these materials promising candidates for various microwave applications [33].

Many techniques have been developed for the measurement of material permittivity. Some general descriptions of those methods are provided in the literature [34,35]. Among these methods, the TE_{011} mode method is superior for the accurate measurement of a microwave dielectric constant for low loss materials with cylindrical shapes [36]. In recent years, the application of dielectric resonators as antennas in a microwave band has been extensively studied due to advantages such as light weight, low cost, small size and low profile [37–39]. DRA can be designed with different shapes to accommodate various design requirements. Moreover, DRA can also be excited with different feeding methods such as probes, microstrip lines, slots and co-planar lines [40]. Among the different DRA shapes, cylindrical DRA offers greater design flexibility where the ratio between the radius to height (r/h) controls the resonance frequency, the quality factor (Q_f) and bandwidth of antennas [41,42]. Although the microwave dielectric properties of $BaZrO_3$ ceramics have been reported in the literature [43–45]. However, their application as DRA has not been explained.

Thus, in this paper, we report on the structural refinement, PL behavior and microwave dielectric properties for possible DRA applications of $BaZrO_3$ ceramics prepared by a solid state reaction method.

2. Experimental procedure

2.1. Synthesis of $BaZrO_3$ ceramics by solid state reaction

$BaZrO_3$ ceramic powder was prepared by the solid state reaction method from reagents barium carbonate ($BaCO_3$) [99, Merck, India Ltd.] and zirconium oxide (ZrO_2) [99, Himedia Laboratories, Mumbai]. The raw materials were stoichiometrically mixed using isopropyl alcohol (IPA) and were milled using an agate mortar to obtain a homogeneous mixture. The ceramic powders were heat-treated at 1250 °C for 2 h and at 1350 °C for 5 h and finally at 1450 °C for 4 h with intermediate grinding and mixing, then dried and granulated with 2 polyvinyl alcohol and pressed to form pellets which were sintered at 1670 °C for 4 h. In all stages, we employed a heating rate 5 °C/min and then furnace cooled at room temperature. The bulk density of the sintered sample determined by the Archimedes method was found to be about 95% of its theoretical density.

2.2. Structural characterizations and optical measurements

These ceramic powders were structurally characterized by XRD patterns recorded on a diffractometer (Rigaku-DMax 2000PC, Japan) using Cu-Kα radiation in the 2θ range from 10° to 70° and 10° to 110° (Rietveld routine) with a scanning rate of 0.02°/min. The Fourier-infrared (FT-IR) absorption spectrum was recorded by the standard KBr pellet technique using a Perkin Elmer FT-IR spectrometer (Spectrum 1000, Japan). Ultraviolet–visible (UV–vis) absorption spectra were taken using a Cary 5G (Varian, USA) spectrophotometer in diffuse reflection mode. PL measurements were performed through a Monospec 27 monochromator (Thermal Jarrel Ash, USA) coupled to a R446 photomultiplier (Hamamatsu, Japan). A krypton ion laser (Coherent Innova 90K, USA) (λ = 350 nm) was used as an excitation source; its maximum output power was kept at 500 mW and a maximum power of 40 mW on the powders after the laser pass through an optical chopper. UV–vis and PL spectra were taken three times for each sample in order to ensure the reliability of the results. All measurements were performed at room temperature.

2.3. Microwave dielectric constant measurements

Microwave dielectric measurements were performed using N5230A (Agilent Technologies, USA) Vector Network Analyzer in a TE_{011}. The dielectric constant (ε_r) was measured using the Hakki–Coleman [42] dielectric resonator method as modified and improved by Courtney [46]. The TE_{011} mode is widely used in materials property characterization because in this mode there is no current crossing the dielectric and the conducting plates, so possible air gaps between the dielectric and the conducting plates have no effects on resonance properties of this mode [47]. The theoretical model is properly described for the configuration mentioned by Courtney and as modified from Kobayashi and Tanaka [48]. The TE_{011} resonance mode has been found most suitable for the real part of the relative dielectric constant (ε_r), and a gain/loss factor ($\tan\delta$) of the specimen was obtained from the measured resonance frequency (f_1) and unloaded quality factor (Q_0) for the TE_{011} resonance mode. The relative dielectric constant and loss factors were calculated from the following formula (1) below [42]:

$$\varepsilon_r = 1 + \left(\frac{c}{\pi D f_1}\right)(\alpha_1^2 + \beta_1^2) \quad (1)$$

where c is the velocity of light, α_1 is given by the mode chart [26] and β_1 is obtained from the resonance frequency (f_1) and the sample dimension. The tan δ is given by Hakki–Coleman [42] as described in Eq. (2):

$$\tan\delta = \frac{A}{Q_u} - BR_s \tag{2}$$

where:

$$A = 1 + \frac{W}{\varepsilon_r} \tag{3}$$

$$B = \left(\frac{l\lambda}{2L}\right)^3 \frac{1+W}{30\pi^2\varepsilon_r l} \tag{4}$$

$$W = \frac{J_1^2(\alpha_1)}{K_1^2(\beta_1)} \cdot \frac{K_0(\beta_1)K_2(\beta_1) - K_1^2(\beta_1)}{J_1^2(\alpha_1) - J_0(\alpha_1)J_2(\alpha_1)} \tag{5}$$

$$R_s = \sqrt{\frac{\pi f_1 \mu}{\sigma}} \tag{6}$$

The function W is the ratio of electric field energy stored on the outside of the rod to the energy inside the rod. The λ is the free-space wavelength and L is the length of the dielectric specimen. The σ is the conductivity of the shorting plate, and Q_0 is the unloaded quality factor of the dielectric resonator. If the dielectric material is isotropic then the characteristic equation for such a resonance structure for the TE_{011} mode is given by Eq. (7):

$$\alpha\frac{J_0(\alpha)}{J_1(\alpha)} = -\beta\frac{K_0(\beta)}{K_1(\beta)} \tag{7}$$

where $J_0(\alpha)$ and $J_1(\alpha)$ are the Bessel functions of the first kind of order zero and one, respectively. $K_0(\beta)$ and $K_1(\beta)$ are the modified Bessel functions of the second kind of orders zero and one, respectively.

Kobayashi and Katoh [49] described a method for the experimental determination of R_s which employs two rod samples cut from the same dielectric rod with equal diameters but different lengths. The rod for a TE_{01l} resonator is "l" times as long as the other rod for a TE_{011} resonator where $l \geq 2$. Here subscripts l and 1 are denoted as quantities for both resonators, respectively. Because of the different conduction loss contributions in the two cases, the modes have almost the same resonance frequency but differ in unloaded Q; i.e if $f_{0l} = f_{01}$, then $Q_{0l} > Q_{01}$. Because both rods have the same (tan δ), the expression for (R_s) is given by Eq. (8) [48]:

$$R_s = 30\pi^2\left(\frac{2L}{l\lambda}\right)^3 \cdot \frac{\varepsilon_r + W}{1+W} \cdot \frac{l}{l-1} \cdot \left(\frac{1}{Q_{01}} - \frac{1}{Q_{0l}}\right) \tag{8}$$

Then substitution of Eq. (8) into Eq. (2) yields:

$$\tan\delta = \frac{A}{l-1}\left(\frac{l}{Q_{0l}} - \frac{1}{Q_{01}}\right) \tag{9}$$

This calculation facilitates the precise measurement of (tan δ). The quality factor ($Q \times f$) was measured using a reflection mode gold-coated copper cavity. Temperature coefficients of the dielectric resonator were measured using a temperature controlled hot plate enclosure with an invar cavity in the temperature range from 30 °C to 60 °C using Eq. (10):

$$\tau_f = \left(\frac{1}{f}\right)\left(\frac{\Delta f}{\Delta T}\right) \tag{10}$$

where $\Delta f/\Delta T$ is the resonance frequency change with respect to temperature.

2.4. Dielectric resonator antenna measurements

An Agilent PNA E8364B network analyzer was employed for measurements. In an experiment introduced by Long et al. [50], DRAs are excited by a wire antenna above a ground plane. The configuration of the two DRAs fabricated from $BaZrO_3$ ceramic materials is shown in Fig. 1.

Each DRA is placed on a conducting ground plane (copper conductor size 5 cm × 5 cm × 2 mm) and excited by a coaxial probe (length = 7 mm). On a practical basis, locating the probe feed adjacent to the DRA is preferred since it does not required drilling into the DRA. The probe adjacent to the DRA can excite the $HE_{11\delta}$ mode which is the basic mode for a cylindrical DRA. The coaxial probe goes through the ground plane and is connected to a SMA connector. The cylindrical DRA depicted in Fig. 1, has a radius (a), height (h) and dielectric constant (ε_r). The probe is located on the x-axis at $x = a$ and $\varphi = 0$.

The cylindrical DRA is worked at the $HE_{11\delta}$ mode whose resonant frequency f_0 can be approximated as [51,52]:

$$f_0 = \frac{2.007}{20\pi\sqrt{\varepsilon_r}}\sqrt{\left(\frac{1.184}{a}\right)^2 + \left(\frac{\pi}{2h}\right)^2} \tag{11}$$

where the f_0 is given in GHz. After obtaining Eq. (11) with the hypothesis that the lateral and upper surfaces of the DRA are perfect magnetic conductors (PMC) which can be verified only for a sample with an infinite permittivity. Therefore, Eq. (11) is the only approximation that leads to an error around 10 [53].

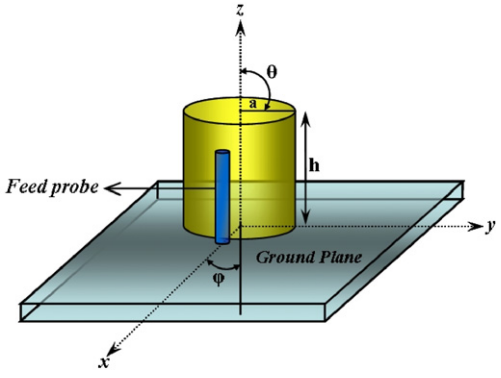

Fig. 1. The geometry of a cylindrical DRA.

A comparison of the values from Eq. (11) to the following closed form of expression for the $HE_{11\delta}$ resonance frequency published in Ref. [37] (see Eq. (12)) is interesting:

$$f = \frac{6.324c}{2\pi a\sqrt{2+\varepsilon_r}}\left(0.27 + 0.36\frac{a}{2h} + 0.02\left(\frac{a}{2h}\right)^2\right) \quad (12)$$

where the f_0 is given in GHz. It is important to note that both experimental and simulation results show large variability of the results according to the probe. This problem finds its origin in the air gap between the DR and metallic conductors and has been thoroughly studied by Junker et al. [54,55].

Radiation Q-factor of the isolated cylindrical DRA can be written as [41,56,57]:

$$Q_{rad} = 0.01007\varepsilon_r^{1.3}\frac{a}{h}\left(1 + 100e^{-2.05\left[0.5\frac{a}{h} - 0.0125\left(\frac{a}{h}\right)^2\right]}\right) \quad (13)$$

The percentage of bandwidth (return loss < -10 dB) is given by Eq. (14) [58].

$$BW\,(\%) = \left(\frac{OR}{CF}\right) \times 100 \quad (14)$$

where BW is the bandwidth, OR is the operating range, and CF is the center frequency.

3. Results and discussion

3.1. XRD patterns and Rietveld refinement analysis

Fig. 2(a and b) shows XRD patterns and Rietveld refinement plot for $BaZrO_3$ ceramic powders sintered at 1670 °C for 4 h, respectively,

As illustrated in Fig. 2(a), XRD patterns indicate that the $BaZrO_3$ ceramic powder is crystalline and structurally ordered at long range. Moreover, we have verified that all XRD peaks of this ceramic correspond to a perovskite-type cubic structure which is in agreement with the respective Inorganic Crystal Structure Database (ICSD) No. 97460 [59]. To confirm that the structure is truly a cubic type, a structural refinement by the Rietveld method was performed [60]. The lattice parameters, unit cell volume and atomic positions were obtained from the ReX Program version 0.6.2 [61]. The structural refinement results for $BaZrO_3$ a ceramic powder sintered at 1670 °C for 4 h are illustrated in Fig. 2(b), and the refinement results are presented in Table 1.

The results shown in Table 1 from the Rietveld refinement method indicate good agreement between XRD patterns observed experimentally and calculated theoretically (Fig. 2(b)). According to the literature [62,63], the quality of the data from structural refinement is generally checked by R-values (R_p, R_{exp}, R_{wp}) and the goodness of fit ($GoF = R_{wp}/R_{exp}$). Moreover, the difference between XRD patterns experimental profiles and calculated data display small differences in the scale of intensity as illustrated by a line ($Y_{Observed} - Y_{Calculated}$).

3.2. Unit cell representations of $BaZrO_3$

Fig. 3 is illustrated a $BaZrO_3$ unit cell.

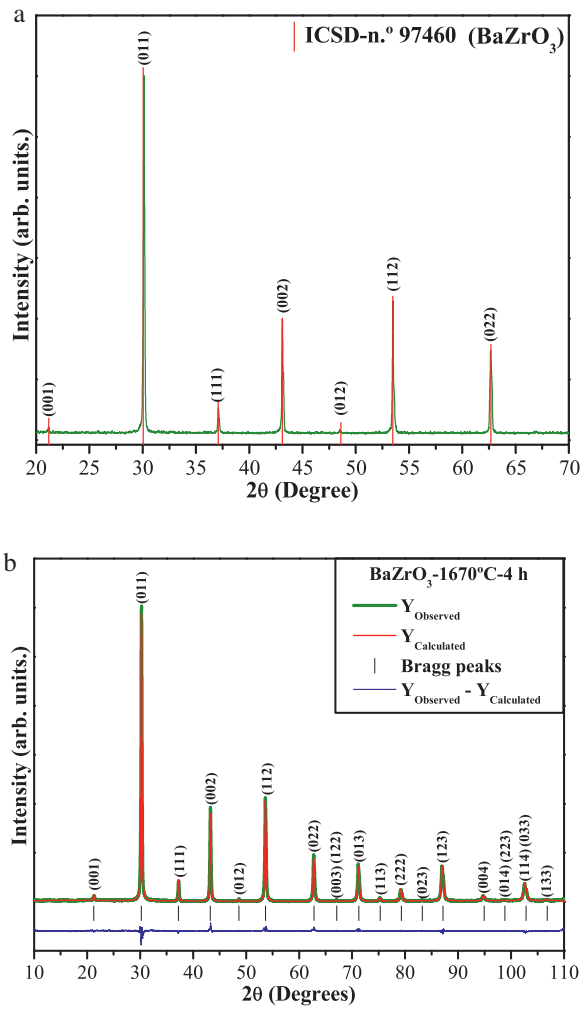

Fig. 2. XRD patterns and structural refinement plot of $BaZrO_3$ ceramics powder, respectively. The vertical dashed lines indicate the position and relative intensity of the respective ICSD Card No. 97460.

This unit cell was modeled through the Visualization for Electronic and Structural Analysis (VESTA) version 2.1.6 for Windows [64] by Rietveld refinement data (lattice parameters and atomic positions) (see Table 1). The $BaZrO_3$ ceramic has a cubic structure with a space group ($Pm\bar{3}m$) and point-group symmetry (O_h). Moreover, zirconium (Zr) atoms (lattice formers) are bonded to six oxygen (O) atoms which form octahedral [ZrO_6] clusters while the barium (Ba) atoms (lattice modifiers) are bonded to twelve O atoms with a cuboctahedral configuration which form [BaO_{12}] clusters. For [ZrO_6] clusters,

Table 1
Lattice parameters, unit cell volume, c/a ratio and atomic position for the $BaZrO_3$ ceramic.

Atoms	Wyckoff	Site	x	y	z	Occupancy
Ba	1*a*	$m-3m$	0	0	0	1
Zr	1*b*	4/*mm* . *m*	0.5	0.5	0.5	1
O1	3*b*	*mm*2 . .	0	0.5	0.5	1

$Pm\bar{3}$m (2 2 1) – cubic ($a = b = c = 4.1812$ Å ; $c/a = 1$; $V = 73.1$ Å^3) $R_p = 9.1$; $R_{wp} = 7.8$; $R_{exp} = 1.2$ and $GoF = 6.5$.

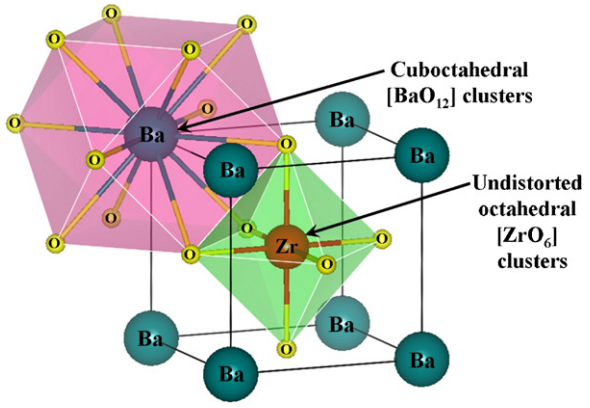

Fig. 3. Schematic representation of a crystalline $BaZrO_3$ (1 × 1 × 1) unit cell which illustrates $[BaO_{12}]$ and $[ZrO_6]$ clusters.

Zr atoms are located in a centrosymmetric position within the octahedron [65].

3.3. Fourier transformed infrared analysis

Fig. 4 shows the FT-IR spectrum of BaZrO3 ceramics. In this Fig. identifies one stronger mode which is found in a specific position at 572 cm^{-1} in the spectrum. According to Ostos et al. [66] and Kumar et al. [67], these IR-active (→ O → Zr → O →) stretching modes which are located at 400–750 cm^{-1} correspond to metal–oxygen stretching vibrations at the B-site of ABO_3 perovskites. Therefore, this band is an anti-symmetric stretch of the $[ZrO_6]$ clusters into the cubic $BaZrO_3$ lattice; these results agree with the literature [68].

3.4. UV–vis absorption spectroscopy analysis

The UV–vis absorbance spectrum of $BaZrO_3$ ceramic powder was recorded at room temperature (see Fig. 5).

The optical band gap energy (E_{gap}) was calculated by a method proposed by Wood and Tauc [69]. According to these

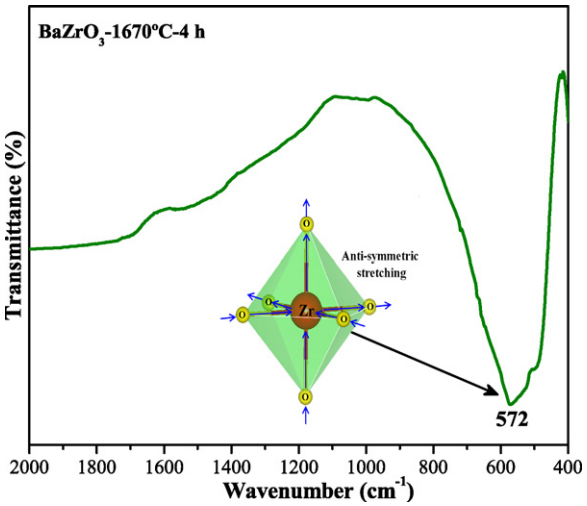

Fig. 4. FT-IR spectrum of $BaZrO_3$ ceramic, and the inset illustrates octahedral $[ZrO_6]$ clusters with anti-symmetric stretching vibration.

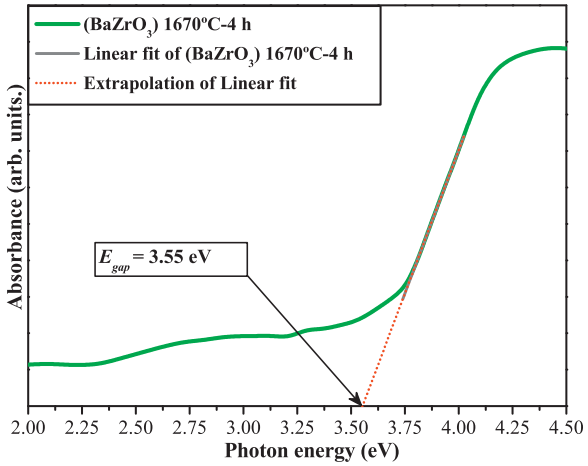

Fig. 5. UV–vis absorbance spectrum of $BaZrO_3$ ceramics.

authors, the optical band gap is associated with absorbance and photon energy by the following equation:

$$h\nu\alpha \propto (h\nu - E_{gap})^n \quad (15)$$

where the exponent (n) depends on the nature of the observed electronic transition, α is the absorbance, h is Planks constant and ν is frequency. For $n = 1/2$, the electronic transition is directly allowed, and the $n = 2$ the transition is indirectly allowed. The E_{gap} value of the $BaZrO_3$ ceramics is evaluated by extrapolating the linear portion of the curve. The value of the exponent "n" is taken to be 2 by considering the allowed indirect transition as suggested by Hou et al. [70]. Again, the studies reported in the literature show that titanates, zirconate–titanate and zirconates with PL properties have an optical absorption process governed by an indirect electronic transition [71–73]. The composition $BaZrO_3$ reveals an optical band gap (E_{gap}) of 3.55 eV. Cavalcante et al. [18] explained theoretically that the optical band gap of a $BaZrO_3$-disorder structure is 3.88 eV which is quite close to our experimental optical band gap value. Therefore, the exponential optical absorption edge and the optical band gap are controlled by the degree of structural order–disorder on the lattice of $BaZrO_3$ powders. In principle, we believe that the E_{gap} value in ceramics is associated with the effect of structural order–disorder in the lattice due to symmetry break between the $[ZrO_6]$–$[ZrO_6]$ and $[BaO_{12}]$–$[BaO_{12}]$ clusters. This symmetry break depends upon the synthesis method as reported in the literature [74]. The solid state synthesis of $BaZrO_3$ causes many intermediary energy (oxygen vacancies) levels due to the repeated cycle of grinding and heating. The intermediary energy levels within the band gap are basically composed of oxygen 2p states situated near the valence band as well as zirconium 4d states located below the conduction band (deep and shallow holes) [74].

3.5. PL emission and wide band model analysis

Fig. 6(a and b) illustrates the PL spectrum at room temperature of $BaZrO_3$ ceramics. The insets are digital photographs for the PL emission of a $BaZrO_3$ ceramics/ deconvolution spectrum and the wide band model composed of

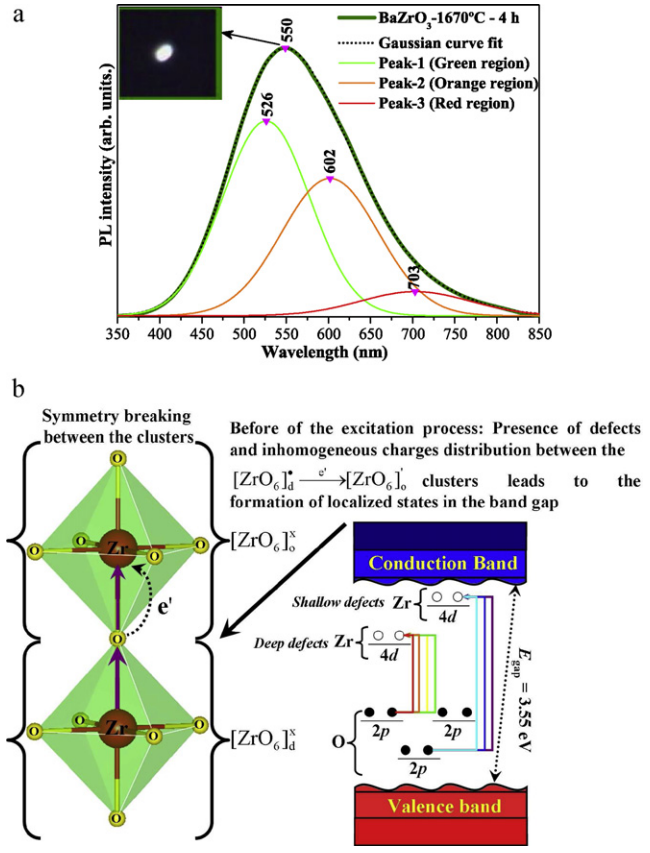

Fig. 6. (a) PL emission spectrum of $BaZrO_3$ ceramics powder and (b) proposed wide band model. Due to excitation process, the material has a symmetry breaking between the $[ZrO_6]$–$[ZrO_6]$ and $[BaO_{12}]$–$[BaO_{12}]$ clusters which promotes a non-homogeneous charge distribution and intermediary (deep and shallow) levels in the gap.

intermediary levels within the band gap as well as the indirect electronic transition process, respectively.

PL spectroscopy is a powerful tool for investigating the levels of structural organization at medium range [75]. The high sensitivity of the PL technique often highlights features which UV–vis absorption measurements rarely define. In particular, PL is a fundamental tool to determine a class of energy levels that are invisible at UV–vis absorption measurements [76,77]. The broad and intense PL emission in the visible green region was observed in $BaZrO_3$ ceramics (see Fig. 6(a) and inset). This PL profile suggests an emission mechanism characterized by the participation of several energy levels or light emission centers which are able to trap electrons within the band gap [77]. Hence, the deconvolution of the PL spectrum was performed to qualitatively estimate the contribution of each individual component in the emission process. The deconvolution was performed through the PeakFit program (4.12 version) using the Voigt area function [78]. The deconvolution results showed that the PL spectrum was better adjusted by three components. Peak-1 located at 526 nm refers to a component with the largest contribution for PL emission in the green region. Peak-2 situated at 602 nm corresponds to a component in the orange region. Peak-3 located at 703 nm is ascribed to a component with a minor contribution for PL emission in the red region. The deconvolution results obtained are shown in Table 2.

Table 2
Results obtained by the deconvolution of the PL spectrum of $BaZrO_3$ ceramics sintered at 1670 °C for 4 h.

Components	Center (nm)	Area peak ()	Region of the visible spectrum
Peak-1	526	51.6	Green
Peak-2	602	40.5	Orange
Peak-3	703	7.9	Red

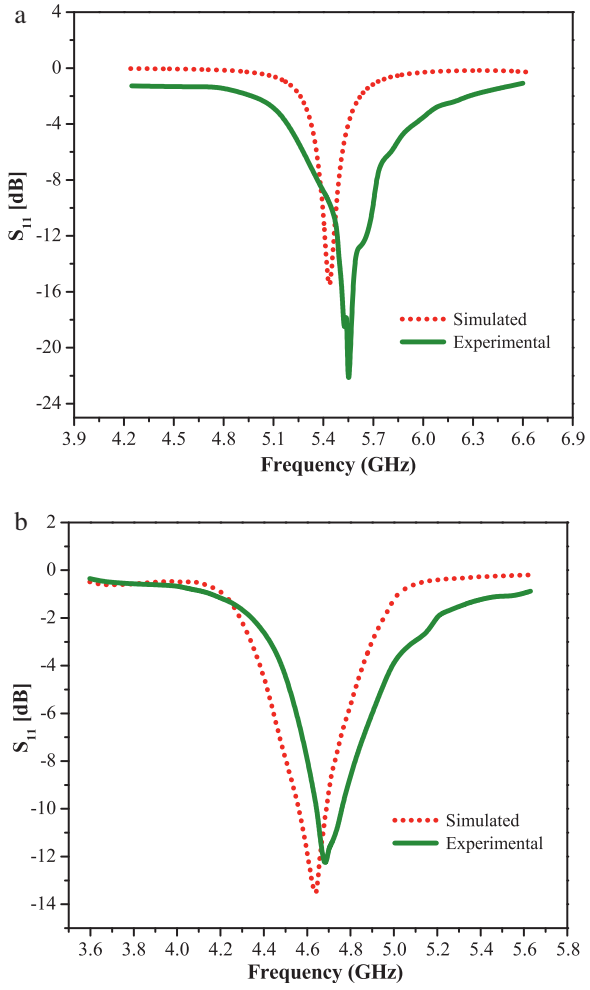

Fig. 7. Measured and simulated return loss vs. frequency of cylindrical DRAs having two different dimensions; (a) $a = 3.715$ mm, $h = 7.22$ mm and (b) $a = 4.91$ mm, $h = 7.85$ mm.

Table 2 illustrates that the smallest area is associated with the component (Peak-3) in the red region. Furthermore, we have observed that the green light component (Peak-1) exhibited the highest area which is predominant in PL behavior. Moreover, the component (Peaks-2) in the orange region is also a considerable contribution in broad PL emission (see Fig. 6(a)). According to the literature [79], the components of PL emission in violet–blue–cyan regions are due to the presence of shallow holes while components in green–yellow–orange–red regions of the visible spectrum are controlled by deep holes within the band gap. Fig. 6(b) verifies that the our proposed wide band model indicates that the origin of the PL

Table 3
Characteristics of the cylindrical dielectric resonator obtained from both experiment and simulation with a dielectric constant of 38.4.

ϵ_r	Radius, a (mm)	Height, h (mm)	Estimated frequency (GHz)	Simulated frequency [HFSS] (GHz)	Experimental frequency (GHz)	Error theoretical frequency ()	Error HFSS ()	Q-factor	Bandwidth percentage
38.4	3.715	7.22	5.89	5.44	5.55	6.12	1.98	35.91	4.51
38.4	4.91	7.85	4.87	4.63	4.68	4.05	1.06	39.15	2.77

behavior in our $BaZrO_3$ ceramic powder is related to deep holes that are responsible for green-orange-red PL emission at room temperature. Therefore, these results suggest that there is a lower contribution of the shallow holes for the PL spectrum (see Fig. 6(b)). Basically, the origin of PL emission in crystalline $BaZrO_3$ powders is possible due to a symmetry break in the lattice. In our wide band model, before the excitation process defects leads to an inhomogeneous charge distribution between the clusters or a pair of electrons (e')–hole ($h^{\bullet}$) [79,80]. These characteristics in the lattice promote the formation of new intermediary levels in the band gap. After this excitation process, numerous electronic transitions across the band gap of this solid induce the emission of photons ($h\nu'$) with lower energy lower than those energy of absorbed photons. Therefore, structural changes can be related to charge polarization in different ranges which are manifestations of quantum confinement when they occur at short and intermediate ranges and are independent of the particle size.

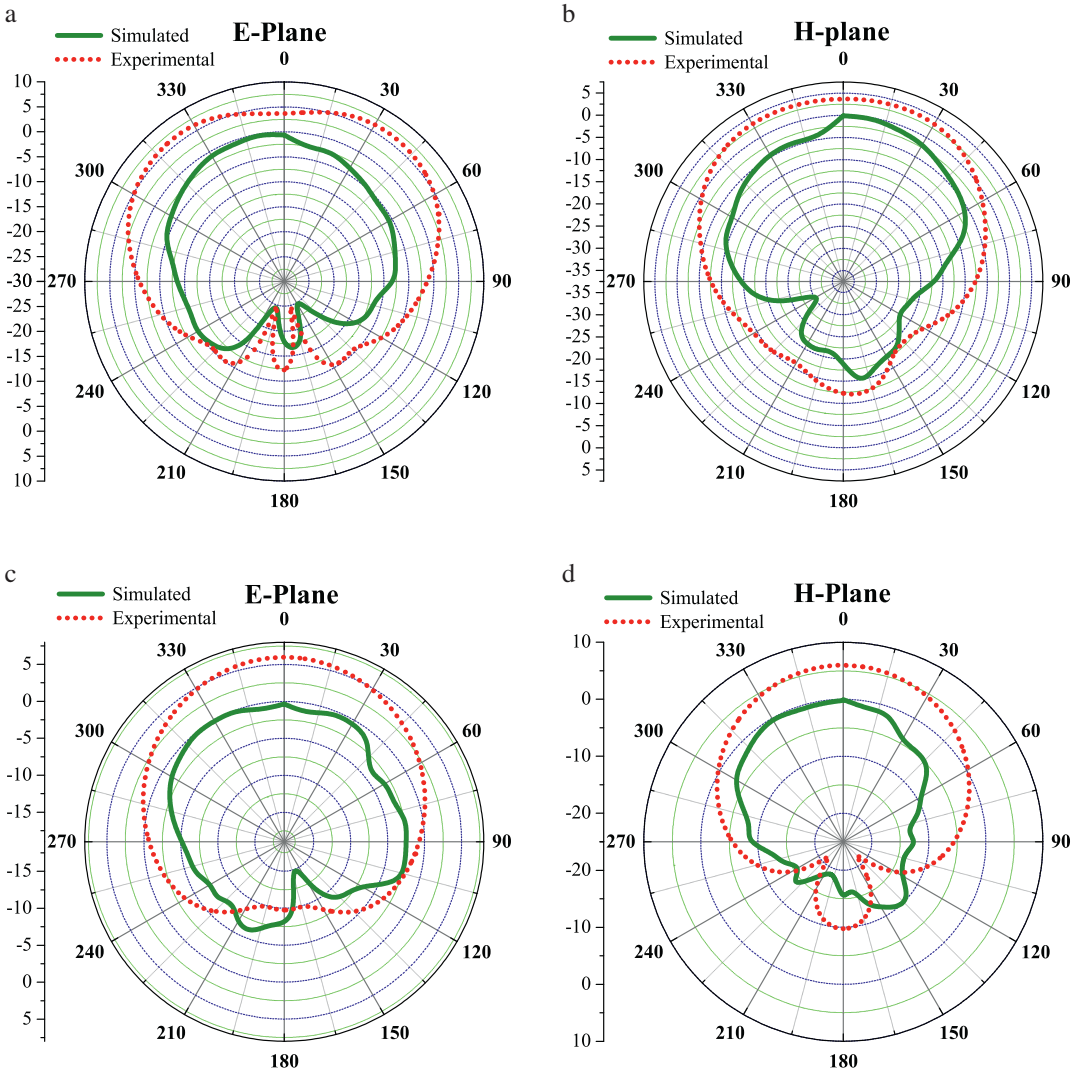

Fig. 8. Radiation patterns of cylindrical dielectric resonators with co-axial feed at 5.55 GHz, and 4.68 GHz; (a and c) elevation pattern and (b and d) Azimuth pattern. Patterns (a) and (b) corresponds to the DRA having a dimension of $a = 3.715$ mm, $h = 7.22$ mm whereas patterns (c) and (d) correspond to the DRA having a dimension of $a = 4.91$ mm, $h = 7.85$ mm.

3.6. Microwave dielectric and dielectric resonator antenna studies of $BaZrO_3$

The microwave dielectric constant of $BaZrO_3$ material was calculated using the Hakki–Coleman dielectric resonator method. The dielectric constant, quality factor values ($Q \times f$) and temperature coefficient at resonance frequency are found to be 38.4, 5731 and 324.35 ppm/°C, respectively. The quality factor ($Q \times f$) is quite smaller than the factor reported in Ref. [81] which might be due to the insertion loss in the sample. The results obtained from the Hakki–Coleman dielectric resonator method were used for the simulation of DRA and are illustrated in Fig. 7(a and b).

The measured return loss and simulated return loss vs. frequency of DRAs having different dimensions are shown in Fig. 7. The estimated resonance frequency, Q-factor and band width percentage of $BaZrO_3$ DRA having two different dimensions are calculated using Eqs. (12), (13) and (14), respectively, and are presented in Table 3. The computed resonance frequency results obtained by HFSS simulations have been found to be in reasonably good agreement with experimental resonance frequency. The difference between experimental and simulated results may be attributed to variations in permittivity, manufacturing tolerance and the frequency excursion caused by the air gap between the probe, resonator and ground plane [82,83] (see Table 3). The resonance frequency of the antenna increases as the size of the DRA decreases; similar behavior has been reported in the literature [84]. The expected resonance frequency can be obtained by suitably choosing the permittivity and size of the antenna. The Q-factor is directly related to the bandwidth of the antenna. The larger the bandwidth, the more coverage over the frequency space that can be utilized by the antenna. The relationship between the Q-factor and the bandwidth is given by Mongia et al. ref. [41] where the Q-factor is inversely related to the bandwidth (see Table 3 and Fig. 8(a–d)).

The radiation characteristics of cylindrical DRA with a coaxial feed are obtained at two different resonance frequencies for two different dimensions (see Fig. 8). The patterns are plotted in both an E-Plane ($\Phi = 0^\circ$ Fig. 8(a,c)) and an H-Plane ($\Phi = 90^\circ$ Fig. 8(b,d)) (experimental H-planes are almost omni-directional). The ideal characteristics of an E-plane should resemble a half-wave dipole pattern parallel to the ground plane. In practice the feeding mechanism may excite more than one mode, so that the patterns differ from the ideal pattern. Moreover, simulation and experimental characteristics at two different frequencies for two different dimensions show some back radiation in the lower half of the plane. The back radiation is more significant in experimental results than in simulated results due to the use of a finite ground plane used in the experimental setup.

4. Conclusions

In summary, $BaZrO_3$ ceramic powder was successfully synthesized by the solid state reaction method at 1670 °C for 4 h. XRD patterns and Rietveld refinement data indicate that this ceramic has a perovskite-type cubic structure with space group ($Pm\bar{3}m$) without a deleterious phase. FT-IR spectrum exhibited a stronger vibrational mode related to their anti-symmetric stretch of [ZrO_6] clusters. UV–vis spectra suggested an indirectly allowed transition with the existence of intermediary energy levels (deep holes) within the band gap. These electronic energy levels are formed mainly by 2p orbitals of oxygen in the valence band VB and 4d orbitals of zirconium in the conduction band. Intense green PL emission at room temperature was observed in $BaZrO_3$ due to presence of deep defects between the valence and conduction band. Two cylindrical DRAs are proposed based on $BaZrO_3$ dielectric materials. The dielectric constant and quality factor were measured by the method proposed by Hakki–Coleman. DRAs have been investigated experimentally and numerically by taking advantage of the configuration of a monopole through an infinite ground plane and using Ansoft's HFSS, respectively. DRA studies show that the resonance frequency and bandwidth not only depend upon the permittivity of the materials, but also depend on the size of materials. The required resonance frequency and bandwidth can be monitored by adjusting the dimension of the same material and can be applicable to different fields of communication. The measurements of DRAs confirm the use of such materials for small DRAs.

Acknowledgements

The Indian authors are pleased to acknowledge Department of Science and Technology, Government of India, New Delhi, for providing financial support through SERC research grant no. SR/S2/CMP-37/2007. The Brazilian authors thank the financial support of the Brazilian Research Financing Institutions: FAPESP-Postdoctorate (No. 2009/50303-4), CNPq and CAPES.

References

[1] Uchino,K. Electrooptic ceramics and their display applications, Ceram. Int. 21 (1995) 309.
[2] Vives,A.A. Piezoelectric Transducers and Applications, 2nd ed., Springer, Berlin, 2008, chapter 15, p. 509.
[3] Sebastian,M.T. Dielectric Materials for Wireless Communication, Elsevier, Amsterdam, 2008, p. 58.
[4] Dong, Z. Ye, T. Zhao, Y. Yu, J. Wang, F. Zhang, L. Wang, X. Guo,S. Perovskite $BaZrO_3$ hollow micro- and nanospheres: controllable fabrication, photoluminescence and adsorption of reactive dyes, J. Mater. Chem. 21 (2011) 5978.
[5] Moreira, M.L. Volanti, D.P. Andrés, J. Montes, P.J.R. Valério, M.E.G. Varela, J.A. Longo,E. Radioluminescence properties of decaoctahedral $BaZrO_3$, Scr. Mater. 64 (2011) 118.
[6] Diaz-Torres, L.A. de la Rosa, E. Oliva, J. Salas, P. Casta no,V.M. BaZrO3:Yb nanophosphor for efficient up-conversion light emission, Prog. Electromagn. Res. Lett. 11 (2009) 139.
[7] Giannici, F. Shirpour, M. Longo, A. Martorana, A. Merkle, R. Maier,J. Long-range and short-range structure of proton-conducting Y:$BaZrO_3$, Chem. Mater. 23 (2011) 2994.
[8] Yamanaka, S. Hamaguchi, T. Oyama, T. Matsuda, T. Kobayashi, S.I. Kurosaki,K. Heat capacities and thermal conductivities of perovskite type $BaZrO_3$ and $BaCeO_3$, J. Alloys Compd. 359 (2003) 1.
[9] Taglieri, G. Tersigni, G. Villa, P.L. Mondelli,C. Synthesis by the citrate route and characterisation of $BaZrO_3$, a high tech ceramic oxide: preliminary results, Int. J. Inorg. Mater. 1 (1999) 103.

[10] Sundell, P.G. Björketun, M.E. Wahnström,G. Thermodynamics of doping and vacancy formation in $BaZrO_3$ perovskite oxide from density functional calculations, Phys. Rev. B 73 (2006) 104112.
[11] Erb, A. Walker, E. Flukiger,R. $BaZrO_3$: the solution for the crucible corrosion problem during the single crystal growth of high-T_c superconductors $REBa_2Cu_3O_{7-\delta}$; RE = Y, Pr, Physica C 245 (1995) 245.
[12] Macario, L.R. Moreira, M.L. Andrés, J. Longo,E. An efficient microwave-assisted hydrothermal synthesis of $BaZrO_3$ microcrystals: growth mechanism and photoluminescence emissions, CrystEngComm 12 (2010) 3612.
[13] Diaz-Torres, L.A. Salas, P. Castaño, V.M. Oliva, J. De la Rosa,E. Chapter 3: nanoparticle synthesis & applications, in: Hydrothermal Synthesis and Photoluminescent Characterization of Nanocrystalline $BaZrO_3$, 2010, p. 361.
[14] Zhou, H. Mao, Y. Wong,S.S. Shape control and spectroscopy of crystalline $BaZrO_3$ perovskite particles, J. Mater. Chem. 17 (2007) 1707.
[15] Moon, C. Nishi, M. Miura, K. Hirao,K. Blue long-lasting phosphorescence of Ti-doped $BaZrO_3$ perovskites, J. Lumin. 129 (2009) 817.
[16] Moreira, M.L. Andrés, J. Varela, J.A. Longo,E. Synthesis of fine micro-sized $BaZrO_3$ powders based on a decaoctahedron shape by the microwave-assisted hydrothermal method, Cryst. Growth Des. 9 (2009) 833.
[17] Oliva, J. De la Rosa, E. Diaz-Torres, L.A. Salas, P. Ángeles-Chavez,C. Annealing effect on the luminescence properties of $BaZrO_3$:Yb^{3+} microcrystals, J. Appl. Phys. 104 (2008) 023505.
[18] Cavalcante, L.S. Longo, V.M. Zampieri, M. Espinosa, J.W.M. Pizani, P.S. Sambrano, J.R. Varela, J.A. Longo, E. Simões, M.L. Paskocimas,C.A. Experimental and theoretical correlation of very intense visible green photoluminescence in $BaZrO_3$ powders, J. Appl. Phys. 103 (2008) 063527.
[19] Cavalcante, L.S. Sczancoski, J.C. Espinosa, J.W.M. Mastelaro, V.R. Michalowicz, A. Pizani, P.S. De Vicente, F.S. Li, M.S. Varela, J.A. Longo,E. Intense blue and green photoluminescence emissions at room temperature in barium zirconate powders, J. Alloys Compd. 471 (2009) 253.
[20] Ye, T. Dong, Z. Zhao, Y. Yu, J. Wang, F. Guo, S. Zou,Y. Controllable synthesis and photoluminescence of single-crystalline $BaHfO_3$ hollow micro- and nanospheres, Langmuir 27 (2011) 8878.
[21] Ye, T. Dong, Z. Zhao, Y. Yu, J. Wang, F. Zhang, L. Zou,Y. Rationally fabricating hollow particles of complex oxides by a templateless hydrothermal route: the case of single-crystalline $SrHfO_3$ hollow cuboidal nanoshells, Dalton Trans. 40 (2011) 2601.
[22] Takahashi, Y. Masai, H. Fujiwara, T. Kitamura, K. Inoue,S. Afterglow in synthetic bazirite, $BaZrSi_3O_9$, J. Ceram. Soc. Jpn. 116 (2008) 357.
[23] Moreira, M.L. Gurgel, M.F.C. Mambrini, G.P. Leite, E.R. Pizani, P.S. Varela, J.A. Longo,E. Photoluminescence of barium titanate and barium zirconate in multilayer disordered thin films at room temperature, J. Phys. Chem. A 112 (2008) 8938.
[24] Guo, L. Wang, X. Zhong, C. Li,L. Preparation and photoluminescence properties of Eu^{3+}-doped $BaZrO_3$ nanotube arrays, J. Am. Ceram. Soc. (2011), doi:10.1111/j. 1551-2916.2011.04741.x.
[25] Gurgel, M.F.C. Moreira, M.L. Paris, E.C. Espinosa, J.W.M. Pizani, P.S. Varela, J.A. Longo,E. $BaZrO_3$ photoluminescence property: an ab-initio analysis of structural deformation and symmetry changes, Int. J. Quantum Chem. 111 (2011) 694.
[26] Moreira, M.L. Buzolin, P.G.C. Longo, V.M. Nicoleti, N.H. Sambrano, J.R. Li, M.S. Varela, J.A. Longo,E. Joint experimental and theoretical analysis of order–disorder effects in cubic $BaZrO_3$ assembled nanoparticles under decaoctahedral shape, J. Phys. Chem. A 115 (2011) 4482.
[27] Swanson, J.R. Rose, V.E. Powell,C.H. Review of international microwave exposure guides, Am. Ind. Hyg. Assoc. J. 31 (1970) 623.
[28] Niehenke, E.C. Pucel, R.A. Bahl,I.J. Microwave and millimeter-wave integrated circuits, IEEE Trans. Microw. Theory Tech. 50 (2002) 846.
[29] Lee, Y.C. Weng, K.W. Lee,W.H. Study on low temperature sintering and microwave dielectric properties of $Ba_2Ti_9O_{20}$-based ceramics, J. Ceram. Soc. Jpn. 117 (2009) 402.
[30] Kaatze,U. Techniques for measuring the microwave dielectric properties of materials, Metrologia 47 (2010) S91.
[31] Bin, L. Aujol, J.F. Gousseau, Y. Ladjal, S. Maitre,H. Resolution-independent characteristic scale dedicated to satellite images, IEEE Trans. Image Process. 16 (2007) 2503.
[32] Bian, J. Liang, Z. Wang,L. Structural evolution and microwave dielectric properties of $Li_{(3-3x)}M_{4x}Nb_{(1-x)}O_4$ (M = M g, Zn; $0 = x = 0.9$), J. Am. Ceram. Soc. 94 (2011) 1447.
[33] Afsar, M.N. Birch, J.R. Clarke,R.N. The measurement of the properties of materials, Proc. IEEE 74 (1986) 183.
[34] Krupka, J. Derzakowski, K. Riddle, B. Baker-Jarvis,J. A dielectric resonator for measurements of complex permittivity of low loss dielectric materials as a function of temperature, Meas. Sci. Technol. 9 (1998) 1751.
[35] Aditya, S. Arokiaswami,A. Microwave measurement instrumentation, in: Wiley Encyclopedia of Electrical and Electronics Engineering Online, Wiley, New York, 1999, p. 185.
[36] Levcheva, V.P. Ivanov,S.A. Application of TE_{011} mode cylindrical resonator for complex permittivity estimation of dielectric materials, Bulg. J. Phys. 32 (2005) 147.
[37] Petosa, A. Ittipiboon, A. Antar, Y.M.M. Roscoe,D. Design and analysis of multisegment dielectric resonator antennas, IEEE Antennas Propag. Mag. 40 (1998) 35.
[38] Luk, K.M. Leung,K.W. Dielectric Resonator Antennas, Research Studies Press Ltd., London, 2003, p. 366.
[39] Antar,Y.M.M. New directions in antenna research using dielectrics, in: Proceeding of the 20th National Radio Science Conference, 2003.
[40] Kumari, R. Behera, S.K.S Behera,S.K.S International Conference on Computational Intelligence and Communication Systems, RGPV Bhopal, 2010.
[41] Mongia, R.K. Bhartia,P. Dielectric resonator antennas: a review and general design relations for resonant frequency and bandwidth, Int. J. Microw. Millimeter-Wave Comput. Aided Eng. 4 (1994) 230.
[42] Hakki, B.W. Coleman,P.D. A dielectric resonator method of measuring inductive capacities in the millimeter range, IRE Trans. Microw. Theory Tech. 8 (1960) 402.
[43] Jiwei, W. Zhiqiang, H. Li, Z. Fangyi,X. Properties of $BaZrO_3$ microwave dielectric ceramic sintered at low temperature with CaO–MgO–SiO_2–B_2O_3 sintering aid, Electron. Comp. Mater. 10 (2010) 12.
[44] Tamura,H. Microwave dielectric losses caused by lattice defects, J. Eur. Ceram. Soc. 26 (2006) 1775.
[45] Shi,F. Influence of $BaZrO_3$, $MnCO_3$ additives on dielectric properties and microstructure of $Ba(Zn_{1/3}Nb_{2/3})O_3$ ceramics and $Ba(Zn_{1/3}Nb_{2/3})O_3$–$Sr(Zn_{1/3}Nb_{2/3})O_3$ solid solutions, Inorg. Mater. 46 (2010) 85.
[46] Courtney,W.E. Analysis and evaluation of a method of measuring the complex permittivity and permeability microwave insulators, IEEE Trans. Microw. Theory Tech. 18 (1970) 476.
[47] Chen, L.F. Ong, C.K. Neo, C.P. Varadan, V.V. Varadan,V.K. Microwave Electronics: Measurement and Materials Characterization, 2004, p. 315.
[48] Kobayashi, Y. Tanaka,S. Resonant modes of a dielectric rod resonator short-circuited at both ends by parallel conducting plates, IEEE Trans. Microw. Theory Tech. 28 (1980) 1077.
[49] Kobayashi, Y. Katoh,M. Microwave measurement of dielectric properties of low-loss materials by the dielectric rod resonator method, IEEE Trans. Microw. Theory Tech. 33 (1985) 586.
[50] Long, S.A. Mcallister, M.W. Shen,L.C. The resonant cylindrical dielectric cavity antenna, IEEE Trans. Antennas Propag. AP-31 (3) (1983) 406.
[51] Luk, K.M. Leung,K.W. Dielectric Resonator Antennas, Research Studies Press Ltd., Baldock, England, 2002.
[52] Kajfez, D. Guillon,P. Dielectric resonators, in: The Artech House Microwave Library Series, 1986.
[53] Almeida, A.F.L. Silva, R.R. Rocha, H.H.B. Fechine, P.B.A. Cavalcanti, F.S.A. Valente, M.A. Freire, F.N.A. Sohn, R.S.T.M. Sombra,A.S.B. Experimental and numerical investigation of a ceramic dielectric resonator (DRA): $CaCu_3Ti_4O_{12}$ (CCTO), Physica B 403 (2008) 586.
[54] Junker, G.P. Glisson, A.W. Kishk,A.A. Input impedance of dielectric resonator antennas top loaded with high permittivity and conducting disks, Microw. Opt. Technol. Lett. 9 (1995) 204.
[55] Junker, G.P. Kishk, A.A. Glisson, A.W. Kajfez,D. Effect of an air gap around the coaxial probe exciting a cylindrical dielectric resonator antenna, Electron. Lett. 30 (1994) 177.

[56] Kishk,A.A. Wideband dielectric resonator antenna in a truncated tetrahedron form excited by a coaxial probe, IEEE Trans. Antennas Propag. 51 (2003) 2907.
[57] Luk, K.M. Leung,K.W. Dielectric Resonator Antennas, Research Studies Press, Hertfordshire, England, 2002.
[58] Grabovickic,R. Accurate calculations of geometrical factors of Hakki–Coleman shielded dielectric resonators, IEEE Trans. Appl. Supercond. 9 (1999) 460.
[59] Pagnier, T. Charrier-Cougoulic, I. Ritter, C. Lucazeau,G. A neutron diffraction study of $BaCe_xZr_{1-x}O_3$, Eur. Phys. J. Appl. Phys. 9 (2000) 1.
[60] Rietveld,H.M. A profile refinement method for nuclear and magnetic structures, J. Appl. Crystallogr. 2 (1967) 65.
[61] Bortolotti, M. Lutterotti, L. Lonardelli,I. J. Appl. Crystallogr. 42 (2009) 538.
[62] Ferrari, M. Lutterotti,L. Method for the simultaneous determination of anisotropic residual stresses and texture by X-ray diffraction, J. Appl. Phys. 76 (1994) 7246.
[63] http://ftp.ccp14.dl.ac.uk/ccp/web-mirrors/lutterotti/.
[64] Momma, K. Izumi,F. VESTA: a three-dimensional visualization system for electronic and structural analysis, J. Appl. Crystallogr. 41 (2008) 653.
[65] Sczancoski, J.C. Cavalcante, L.S. Badapanda, T. Rout, S.K. Panigrahi, S. Mastelaro, V.R. Varela, J.A. Siu Li, M. Longo,E. Structure and optical properties of $[Ba_{1-x}Y_{2x/3}](Zr_{0.25}Ti_{0.75})O_3$ powders, Solid State Sci. 12 (2010) 1160.
[66] Ostos, C. Mestres, L. Martinez-Sarrion, M.L. Garcia, J.E. Albareda, A. Perez,R. Synthesis and characterization of A-site deficient rare-earth doped $BaZr_xTi_{1-x}O_3$ perovskite-type compounds, Solid State Sci. 11 (2009) 1016.
[67] Kumar, H.P. Vijayakumar, C. George, C.N. Solomon, S. Jose, R. Thomas, J.K. Koshy,J. Characterization and sintering of $BaZrO_3$ nanoparticles synthesized through a single-step combustion process, J. Alloys Compd. 458 (2008) 528.
[68] Su, B. Choy,K.L. Structure and growth characteristics of $BaZrO_3$ films produced using an electrostatic assisted aerosol–gel deposition method, J. Mater. Chem. 9 (1999) 1629.
[69] Wood, D.L. Tauc,J. Weak absorption tails in amorphous semiconductors, Phys. Rev. B 5 (1972) 3144.
[70] Huo, M. Fu, C.L. Guo, Q. Liao, H. Deng, X.L. Zhang,C.Y. First-principle study on electronic structures of barium zirconate titanate (BZT), J. Funct. Mater. 42 (2011) 877.
[71] Gurgel, M.F.C. Espinosa, J.W.M. Campos, A.B. Rosa, I.L.V. Joya, M.R. Souza, A.G. Zaguete, M.A. Pizani, P.S. Leite, E.R. Varela,J.A. Photoluminescence of crystalline and disordered BTO:Mn powder: experimental and theoretical modeling, J. Lumin. 126 (2007) 771.
[72] Cavalcante, L.S. Gurgel, M.F.C. Paris, E.C. Sim oes, A.Z. Joya, M.R. Varela, J.A. Pizani, P.S. Longo,E. Combined experimental and theoretical investigations of the photoluminescent behavior of $Ba(Ti,Zr)O_3$ thin films, Acta Mater. 55 (2007) 6416.
[73] Longo, V.M. Cavalcante, L.S. Erlo, R. Mastelaro, V.R. de Figueiredo, A.T. Sambrano, J.R. de Lazaro, S. Freitas, A.Z. Gomes, L. Vieira, N.D. Jr., Varela, J.A. Longo,E. Strong violet-blue light photoluminescence emission at room temperature in $SrZrO_3$: joint experimental and theoretical study, Acta Mater. 56 (2007) 2191.
[74] Badapanda, T. Rout, S.K. Cavalcante, L.S. Sczancoski, J.C. Panigrahi, S. Longo, E. Siu Li,M. Optical and dielectric relaxor behaviour of Ba(Zr0.25Ti0.75)O3 ceramic explained by means of distorted clusters, J. Phys. D: Appl. Phys. 42 (2009) 175414.
[75] Montoncello, F. Carotta, M.C. Cavicchi, B. Ferroni, M. Giberti, A. Guidi, V. Malagú, C. Martinelli, G. Meinardi,F. Near-infrared photoluminescence in titania: evidence for phonon-replica effect, J. Appl. Phys. 94 (2003) 1501.
[76] Longo, V.M. Cavalcante, L.S. de Figueiredo, A.T. Santos, L.P.S. Longo, E. Varela, J.A. Sambrano, J.R. Paskocimas, C.A. De Vicente, F.S. Hernandes,A.C. Highly intense violet-blue light emission at room temperature in structurally disordered $SrZrO_3$ powders, Appl. Phys. Lett. 90 (2007) 091906.
[77] Rout, S.K. Cavalcante, L.S. Sczancoski, J.C. Badapanda, T. Panigrahi, S. Li, M.S. Longo,E. Photoluminescence property of $Ba(Zr_{0.25}Ti_{0.75})O_3$ powders prepared by solid state reaction and polymeric precursor method, Physica B 404 (2009) 3341.
[78] http://www.sigmaplot.com/products/peakfit/peakfit.php.
[79] Cavalcante, L.S. Sczancoski, J.C. De Vicente, F.S. Frabbro, M.T. Siu Li, M. Varela, J.A. Longo,E. Microstructure, dielectric properties and optical band gap control on the photoluminescence behavior of $Ba[Zr_{0.25}Ti_{0.75}]O_3$ thin films, J. Sol–Gel Sci. Technol. 49 (2009) 35.
[80] Vikhnin, V.S. Kaplyanskii, A.A. Kutsenko, A.B. Liu, G.K. Beitz, J.V. Kapphan,S.E. ‘‘Charge transfer-lattice’’ clusters induced by charged impurities, J. Lumin. 94-95 (1999) 775–779.
[81] Sivasubramanyan, V. Murthy, V.R.K. Viswanathan,B. Microwave dielectric properties of certain simple alkaline earth perovskite compounds as a function of tolerance factor, Jpn. J. Appl. Phys. 36 (1997) 194.
[82] Junker, G.P. Kishk, A.A. Glisson, A.W. Kajfez,D. Effect of an air gap on a cylindrical dielectric resonator antennas operating in the TM mode, Electron. Lett. 30 (1994) 97.
[83] Junker, G.P. Kishk, A.A. Glisson, A.W. Kajfez,D. The effect of fabrication imperfections for ground-plane-backed coaxial probe fed dielectric resonator antennas, IEEE Antennas Propag. Mag. 37 (1995) 40.
[84] Peng, Z. Wang, H. Xi Yao, Dielectric resonator antennas using high permittivity ceramics, Ceram. Int. 30 (2004) 1211.